**Proceedings of ASME Turbo Expo 2009: Power for Land, Sea and Air**
**GT2009**
**June 8-12, 2009, Orlando, Florida, USA**

# GT2009-59925

# EXPERIMENTAL INVESTIGATION OF TURNING FLOW EFFECTS ON INNOVATIVE TRAILING EDGE COOLING CONFIGURATIONS WITH ENLARGED PEDESTALS AND SQUARE OR SEMICIRCULAR RIBS

**Bruno Facchini, Francesco Simonetti, Lorenzo Tarchi**
Department of Energy Engineering "Sergio Stecco"
Via Santa Marta, 3 - 50139 Firenze, ITALY
Email: lorenzo.tarchi@htc.de.unifi.it, WWW: http://www.htc.de.unifi.it

## ABSTRACT

In this paper the experimental measurements concerning the heat transfer capabilities of several trailing edge (TE) cooling configurations that are based on the combination of enlarged pedestals and small rib turbulators are presented. The baseline geometry consists of a converging duct, reproducing the typical shape of a high pressure turbine blade TE, with two rows of enlarged pedestals. Three rows of square or semicircular turbulators were arranged in between the pedestals on the pressure side (PS) surface; the ribs height is $e = 1\,mm$ and the pitch is $P/e = 10$. The airflow pattern inside the test rig simulates the rotor blade cooling scheme with a 90deg turning flow from the hub inlet to the TE outlet. For each configuration heat transfer measurements were made keeping Mach number fixed at 0.3 and varying Reynolds number from 9000 to 27000 in the TE throat section. The effect of a varying tip massflow rate was tested considering 0%, 12.5% and 25% of the TE massflow. The detailed HTC maps were measured using the transient technique with TLC and a PMMA test article.

As expected, by comparison with the baseline geometry, test results show that the HTC distribution and the average Nusselt number over the PS surface are affected by the presence of the ribs which promote the airstream turbulence. However, no remarkable difference between the results from different rib shapes can be highlighted. The tip massflow rate alters the HTC distribution in the radial direction over the whole TE. The results are compared with previous experiments, performed on the same geometries, but with an axial inlet.

## Nomenclature

| | | |
|---|---|---|
| $\overline{h}$ | Averaged Heat Transfer Coefficient | $[W/(m^2K)]$ |
| $D$ | Diameter | $[m]$ |
| $f$ | Friction Factor | |
| $k$ | Thermal Conductivity | $[W/(m \cdot K)]$ |
| $Ma$ | Mach Number | |
| $Nu$ | Nusselt Number | |
| $P$ | Rib Pitch | [m] |
| $p$ | Pressure | [Pa] |
| $Pr$ | Prandtl Number | |
| $Re$ | Reynolds Number | |
| $RF$ | Recovery Factor | |
| $T$ | Temperature | $[K]$ |
| $v$ | Velocity | $[m/s]$ |

**Acronyms**

| | |
|---|---|
| $HTC$ | Heat Transfer Coefficient |
| $L0$ | Inlet Region |
| $L1$ | Converging Region |
| $L2$ | Constant Height Region |
| $PMMA$ | Polymethyl methacrylate |
| $PS$ | Pressure Side |
| $TC$ | Thermocouple |
| $TE$ | Trailing Edge |
| $TLC$ | Thermo-chromic Liquid Crystals |

**Greeks**

| | | |
|---|---|---|
| $\alpha$ | Thermocouple Recovery Factor | |
| $\gamma$ | Specific Heats Ratio | |
| $\rho$ | Density | $[kg/m^3]$ |

**Subscripts**

| | |
|---|---|
| 0 | Total |
| *h* | Hydraulic |
| *s* | Static |

## INTRODUCTION

The main goal of current research in the aero engine and gas turbine industry is the achievement of higher thrust/weight ratio of the gas turbines and the reduction of the fuel consumption. For these purposes, the improvement of thermodynamic performance is generally obtained by increasing the operating temperature, i.e. the Turbine Inlet Temperature. However, available materials for turbine blades cannot withstand the required high temperatures due to the degradation of structural strength.

To maintain and prolong structural integrity and to reduce maintenance costs it is necessary to develop very efficient cooling systems and employ thermal barrier coatings or high-resistance materials that improve strength in the presence of high thermal stresses.

Blade cooling is achieved by combining external and internal systems. For internal cooling strategies, heat transfer is augmented by encouraging increased turbulence levels. To increase aerodynamic efficiency, blades are generally manufactured with very thin trailing edge (TE) profiles, so the design of efficient cooling systems requires a set of turbulators to maintain the surface temperature under critical values due to the reduction of the ducts area and the increase of the aspect ratio.

Thus, the coolant system must adequately tradeoff increased heat transfer rates and minimal pressure loss.

Typical TE configurations consist of some inserts of various shape placed in a slightly convergent duct; such elements, generally named pedestals, are circular or oblong pin fins. They cause an increase in heat transfer and serve also as structural devices. The use of pin fin arrays is one of the best choices to enhance overall heat transfer coefficient (HTC) of the coolant side in the TE zone where, especially in aeroengine blades, impingement or multi-pass channels with ribs cannot be accommodated due to manufacturing constraints [1]. Compared to multirow pin fins, enlarged pedestal arrays decrease pressure drop but heat transfer augmentation is limited.

In recent years, Hwang and Lui [2], Carcasci et al. [3] and Facchini et al. [4] performed experimental analysis about pedestals in a converging duct. They showed the effect of an accelerating flow both on heat transfer and on pressure drop in specific trailing edge cooling geometries.

Rib turbulators are usually employed to enhance heat transfer of internal channels. Extensive experimental studies about ribs were performed by Han et al. [5], Han [6] and Han and Park [7]. They proposed a semi-empirical correlation for fully developed flow into a ribbed channel taking into account geometric and flow conditions. Chandra and Cook [8] and Chandra et al. [9] studied the effects of the number of ribbed walls on heat transfer and friction factor in rectangular ribbed duct.

The effect of the shape of the ribs on the heat transfer and the pressure drop was investigated by Taslim and Spring [10], Taslim and Nezym [11], Burggraf [12], Han et Chandra. [13]. The rib geometries were tested in ducts with different positioning, i.e. on one or two walls of the duct, with different area blockages and spacing. Generally, the results showed that ribs with square edges enhance the heat transfer because they promote the turbulence of the airstream. However, the ribs with rounded edges have lower pressure losses. The comparison of the global performances of the ribs was also affected by the height, pitch and area blockage.

In recent years, several flowfield visualizations of rib-roughened ducts have been performed. Cakan and Arts [14] performed Digital Particle Image Velocimetry (DPIV) measurements, showing that the flow inside the channel is characterized by a series of accelerations, reattachments and redevelopments due to the sudden changes in cross section and each rib also produces a recirculating region upstream of it. Moreover, secondary flow vortices were generated. Flowfield visualizations have been also performed by Kiml et al. [15] and Liou et al. [16] using the Particle Image Velocimetry (PIV) and the Laser Doppler Velocimetry (LDV) techniques; they showed that the number of rib-roughened walls and the arrangement of the turbulators influenced secondary flow structure, the recirculation size and the position of flow reattachments downstream the rib rows. These effects directly affected the heat transfer coefficient values and distribution.

As stated, in technical literature there is a large number of experimental investigations concerning the heat transfer of rib-roughened ducts taking into account for duct and rib shape and turbulators disposition, but tests were mainly addressed to gain knowledge on axial configurations. Thus, in recent years efforts have been addressed to investigate the combined effect of channel shape and coolant stream orientation to take into account for the real internal TE flow configuration.

Hwang and Lui [17] compared experimental results of straight and 90*deg* turned trapezoidal ducts for geometries consisting of circular pin fins. Data comparison showed a significant influence of coolant flow orientation and also channel shape on pressure drop and mainly on HTC distribution, due to the separated flow structures arising with turned flow. A similar strong influence of coolant orientation and channel shape was found by Kulasekharan and Prasad [18] who also performed a wide numerical investigation, testing the effects of flow orientation, channel shape (straight and cambered mean line) and channel section shape (rectangular and converged). Again, results showed HTC sensitivity to test case geometry design, even though effects were different to those of Hwang and Lui [17]. Recent advancements in test rig design were presented by Liu et al. [19], who set up a rotating test rig reproducing a converging TE channel to take

into account the discharging of coolant through TE slots. In such a geometry, the effect of rotation on HTC was discussed finding a relation between rotation number and Nu.

Concerning the experimental techniques, Wang et al. [20,21] performed detailed heat transfer measurements on the surface of pedestals array with TLC transient technique; with the same experimental method Hwang et al. [2, 17, 22] evaluated heat transfer and pressure drop in trailing edge cooling geometries typical of real blades: wedge and trapezoidal ducts, pin shape and lateral flow effects were investigated. Lately, Facchini et al. [4, 23] besides the surface HTC measurements with TLC, evaluated pedestal contribution to heat transfer using high conductivity inserts and an inverse data reduction method based on a finite element simulation of the transient test, showing that pedestals have higher HTC than the surrounding surface. On the contrary, Chen et al. [24] using the lumped heat capacitance method to estimate the pin fin contribution, measured lower heat transfer values over the pin fin surface.

In the present article, to investigate the heat transfer of the internal trailing edge section in a more realistic way, a TE configuration was tested taking into account the effect of both radial and axial coolant flows with tip and trailing edge massflow rates. The baseline geometry consists of two enlarged pedestal arrays with and without fillet radius arranged in a wedged shape duct and three rows of square or semicircular ribs placed in between the first array of pedestals. The effects of square and semicircular ribs were investigated in order to understand how a possible manufacturing defect (i.e. a rounded rib instead of a square one) could affect the cooling performance of the system, considering high-blockage ribs.

A heat transfer experimental survey was performed using a transient technique that allowed to measure detailed two dimensional HTC maps over the PS surface. Along with heat transfer survey, pressure drop has been investigated for all the tested conditions. The tests were performed considering $Re = 9000 - 18000 - 27000$ at a fixed $Ma = 0.3$ in the TE throat section; these values are close to the operational conditions of the real high pressure gas turbine blades.

Results from mixed axial-radial configurations were also compared with axial flow configuration of the test article data.

The experimental investigation on axial geometries was done by Facchini and Tarchi [25]. Concerning the combined effect of enlarged pedestals and rib turbulators in a wedge shaped duct Bacci et al. [26] and Di Carmine et al. [27] discussed results from numerical investigations referring to the axial configurations of geometries presented in this article in terms of heat transfer, flow field and pressure drop.

## EXPERIMENTS

### Test Facility

The experimental survey was performed at the Department of Energy Engineering of the University of Florence. The final aim of this activity is the measurement of the HTC over the internal surfaces of three different geometries using a transient technique. The test rig, presented in Fig. 1, consists of a suction-type

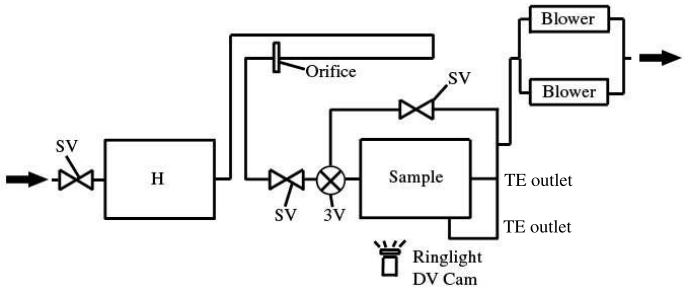


Figure 1. EXPERIMENTAL SETUP

circuit that allows complete control of the air stream in terms of both temperature and massflow rate. The mainstream air passes through a $9.0\,kW$ electronically controlled electric heater ($H$ in Fig. 1); then, the flow rate is measured by an orifice and the flow conditions, in terms of pressure and massflow rate can be modified through the valves ($SV$) in the the test rig. A three way valve ($3V$) with a pneumatic actuator ensures that the sample was at room temperature, as required by the transient technique, while the other components of the test rig are warming up. Two rotary vane vacuum pumps, powered by two $7.5\,kW$ electric motors, provide the suction for a maximum massflow rate of $0.10\,kg/s$. Vacuum conditions are required in such a way that Mach and Reynolds numbers are those typical of the real engines. The air temperature is controlled by means of a four wire Resistance Temperature Detector (Pt100); two pressure scanners Scanivalve® DSA 3017 with temperature compensated piezoresistive relative pressure sensors allowed us to measure the total or static pressure in 32 different locations with an accuracy of $6.9\,Pa$. Several T-type thermocouples connected to a data acquisition/switch unit (HP-Agilent® 34970A) measured the mainstream temperature and the aluminum pedestal temperature. A digital three-charge-coupled-device (3CCD) camcorder (Canon® XM-2) records a sequence of color bitmap images ($720 \times 576$ pixel, 25 frames/s) from the TLC painted surface on a PC (IEEE-1394 standard). The illuminating system (Schott-Fostec® KL1500 LCD) uses an optical fiber ring light to ensure a uniform illumination on the test surface, and it allows to keep both color temperature and light intensity constant. In order to reduce any undesired PMMA reflections, two polarized lens filters are fitted on both ring light and camcorder lenses. Encapsu-

lated TLCs are the devices used to evaluate surface temperature and, consequently, the heat transfer coefficient. For our purpose, we used the 40C1W formulation of Hallcrest® active from $40°C$ to $41°C$. Crystals are thinned with water and sprayed with an airbrush on the test surface, then a black background paint is applied. TLCs have been calibrated, replicating the same optic conditions of the real test (i.e. with the camera perpendicular to the TLC sheet): the green color peak intensity was found at $41.23°C$ and it is the most repeatable and evident effect, so it was used as temperature reference in the data reduction procedure.

## Geometries

Geometries studied in this paper, presented in Fig. 2, allow the investigation of the combined effect of enlarged pedestal and ribs, considering the axial redirection of the inlet radial flow.

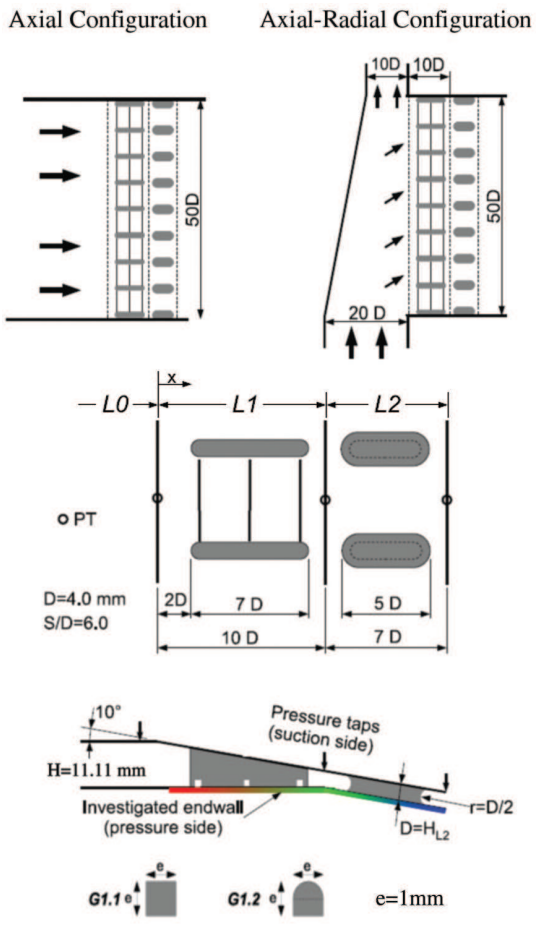


Figure 2. AXIAL AND AXIAL-RADIAL GEOMETRIES

In order to better understand the effects of rib turbulators on heat transfer and pressure loss, we considered a baseline geometry, $G1.0$. This geometry consists of two arrays of enlarged pedestals, placed in a variable height duct; the second row, placed in region $L2$ inline with the first one, has a fillet radius ($r = D/2$).

In the investigated configuration the flow enters in radial direction from a smooth duct $20D$ wide, with constant height, reproducing the flow path of a typical rotor trailing edge configuration. Then the flow turns in axial direction entering in the $L1$ region or leaves $L0$ in radial direction across a $10D$ wide constant height smooth duct. A redirecting device produces a linear reduction of the radial duct width up to the tip section from $20D$ ($80\,mm$) to $10D$ ($40\,mm$), while the height remains constant, $H_{L0} = 11.11\,mm$. A square mesh grid located upstream the entrance ensures a 4% turbulence level at the outlet of the $20D$ wide duct.

The three rows of turbulators are placed on the PS surface, equi-spaced in between the first array of pedestal in the $L1$ region. The first rib axis is placed $1D$ downstream of the pedestal leading edge, the rib height is fixed ($e = 1\,mm$) and pitch is ten times the height ($P/e = 10$, $e/H_{L2} = 0.25$). Two different shapes were investigated: square ($G1.1$) and semicircular ($G1.2$), both with the same height, see Fig. 2.

Test results were also compared to previous results performed on similar geometries arranged in an axial configuration [25]; the two test articles differ from each other only in the inlet region $L0$, while are exactly the same in $L1$ and $L2$. In fact in the axial configuration the entrance region ($L0$) consists of a $11.11 \times 200\,mm$ smooth constant height duct; the aforementioned test articles are compared in Fig. 2.

Models are made of transparent PMMA and TLC were sprayed over the whole PS surface from $L0$ to $L2$, including the hub inlet and the tip outlet regions. Air temperature is measured at the $L0$ region inlet in the axial model and in the hub inlet in the axial-radial model with two miniaturized thermocouples allowing the required fast response for transient tests. As regards pressure measurements, static pressure is measured by seven pressure taps on the suction side, from L0 to L2 and additional taps are located in the hub inlet and tip outlet ducts.

## Experimental Procedure

Heat transfer tests were performed using a combined transient technique that allowed the measurement of HTC on the pressure side surface with a transient test. During the warm up of the rig, the test model was kept at constant temperature. When air temperature reached about $70 - 80°C$ in the by-pass circuit, the 3-way valve was switched making the air passing through the test model; automatically air temperature and pressure values were recorded and the camcorder started acquiring frames of the TLC coated surface. Transient test ended when the liquid crystal reaches the end of the activation range over the whole surface.

Pressure loss was evaluated with a cold test.

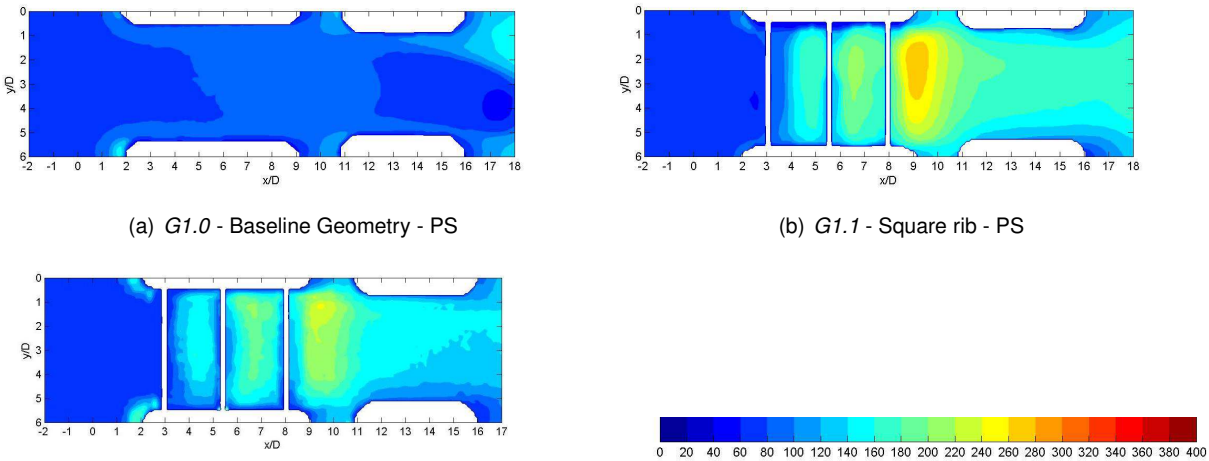


(a) *G1.0* - Baseline Geometry - PS

(b) *G1.1* - Square rib - PS

(c) *G1.2* - Semicircular rib - PS

(d) $W/(m^2K)$

Figure 3. ENDWALL HEAT TRANSFER COEFFICIENT MAPS - AXIAL CONFIGURATION - $Re = 18000$ [25]

## DATA REDUCTION

### Reynolds and Nusselt Number Definition

Reynolds and Nusselt numbers for data reduction of tested geometries are based on the $L1$ inlet section ($x = 0$); this rule was also applied for the axial configuration of the test rig [25].

$$Re = \frac{\dot{m}\, D_{L1inlet}}{A_{L1inlet}\, \mu} \qquad Nu = \frac{\overline{h}\, D_{L1inlet}}{k} \tag{1}$$

where $\dot{m}$ is the massflow rate flowing through the TE, $D_{L1inlet}$ is the hydraulic diameter of the reference duct with cross section area $A_{L1inlet} = 11.11 \times 200\, mm^2$. $\mu$ and $k$ were evaluated at the flow total temperature $T_0$ in the $L0$ inlet region. $\overline{h}$ is averaged value of the HTC over the PS surface of the regions $L0$, $L1$ or $L2$.

$$T_0 = T_{TC}\frac{1+\frac{\gamma-1}{2}Ma^2}{1+\alpha\frac{\gamma-1}{2}Ma^2} \qquad \alpha = \frac{T_{TC}-T_s}{T_0-T_s} \tag{2}$$

where $T_{TC}$ is the temperature measured by the thermocouples, $\alpha$ the recovery factor of the thermocouples dependent upon the used thermocouples and $T_s$ is the static temperature of the fluid. $T_s$ can be calculated from the definition of $\alpha$ given in Eq. 2 for $Ma < 0.3$.

In *L1* region, where duct height decreases and consequently the air velocity rapidly increases, the local adiabatic wall temperature was calculated considering the local Mach number, that was assumed as the averaged $Ma$ along the spanwise direction.

Morevover, to calculate the necessary flow properties in the region $L1$, an iterative procedure was developed to obtain the local bulk temperature $T_{L1}$ from $T_0$ (see Eq. 2). Iterations are necessary because in Eq. 2 $T_{L1}$ depends on the mean Mach number, which in turn depends on $T_{L1}$, as the recovery factor for turbulent flows [28]:

$$T_{L1} = \frac{T_0}{1+RF\frac{\gamma-1}{2}Ma^2} \qquad RF = Pr^{1/3}\ \text{(turbulent flow)} \tag{3}$$

$T_{L1}$ was then used as bulk temperature for the evaluation of the heat transfer coefficient.

### Heat Transfer Coefficient Evaluation

Detailed heat transfer coefficient distribution on the PS surface is obtained assuming one dimensional conduction over a semi-infinite solid [29, 30] and using the bulk temperature calculated with Eq.3. The *Series of Steps* method [31] was implemented to take into account air temperature time history.

### Pressure Drop Evaluation

As previously explained, pressure taps have been arranged starting from the inlet of $L1$ until the end of $L2$ region, at the center of the hub inlet and tip outlet sections (Fig. 2).

The pressure drop were used to define a friction factor $f$ as:

$$f = \frac{\Delta p_0}{\frac{1}{2}\rho_{TEoutlet} v^2_{TEoutlet}} \tag{4}$$

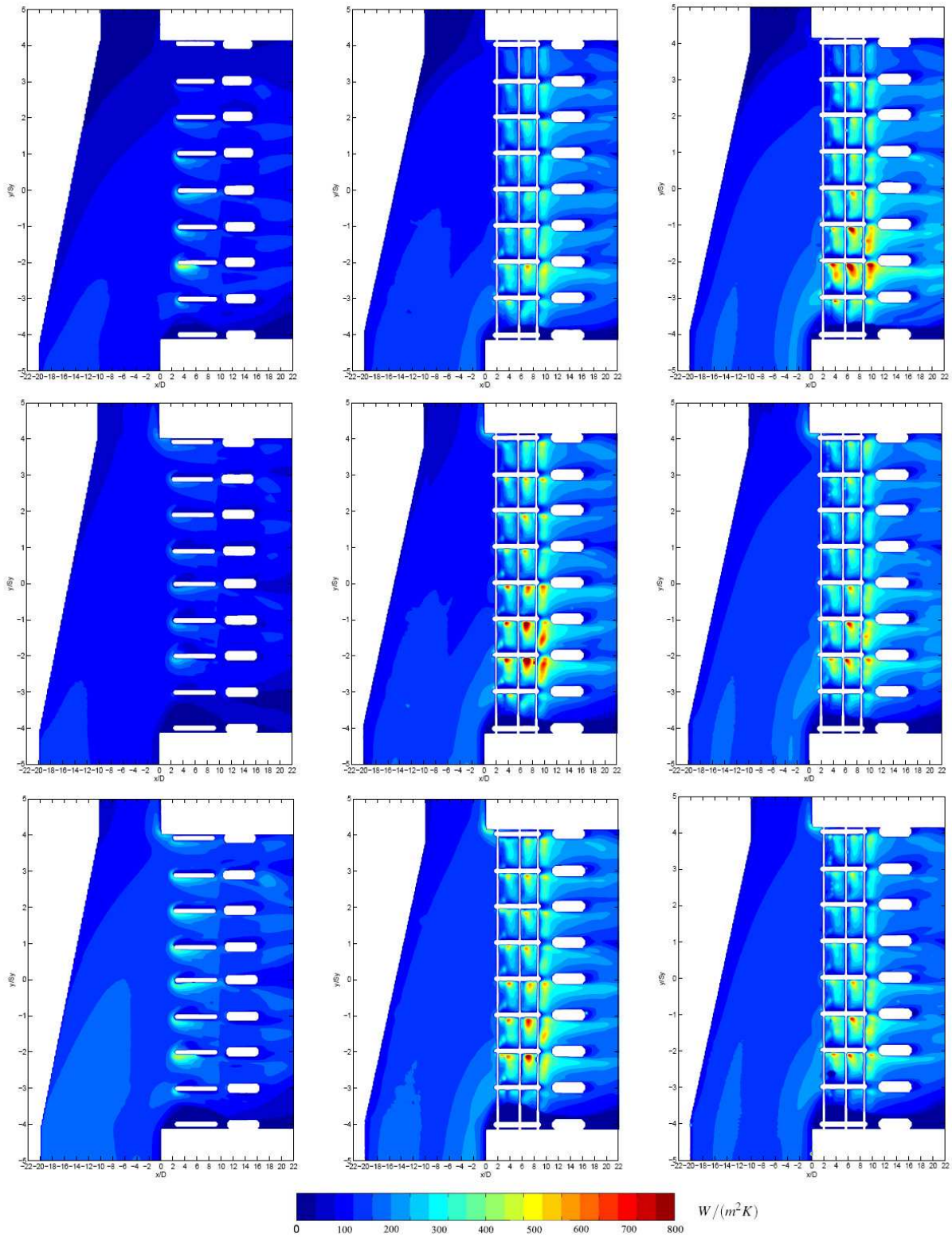


Figure 4. PS SURFACE HEAT TRANSFER COEFFICIENT MAPS - AXIAL-RADIAL CONFIGURATIONS - $Re = 18000$

where $\Delta p_0$ is the total pressure difference between the hub inlet and $L2$ outlet (that corresponds to $x/D = 17$) sections. The dynamic pressure was obtained calculating the density from the measured pressure and temperature and the velocity from the massflow rate measured at the outlet of TE. Total pressure was calculated adding the dynamic pressure to the average static pressure of each section. The effect of density variations was taken into account only in the TE throat section where $Ma = 0.3$, while $Ma$ is lower in the region $L1$.

### Experimental Uncertainty

The uncertainty analysis was performed following the standard [32] based on the Kline and McClintock method [33]. Typical uncertainties of the most important parameters are: $HTC = 12.2\%$, $Re = 2.8\%$, $f = 5.4\%$. More details about the individual contributions to the uncertainties of the single parameters for each of the measured physical properties are reported by Facchini et al. [4] for the same flow conditions of the present results.

## EXPERIMENTAL RESULTS

Three tests were performed with no air stream flowing through the tip outlet, varying the Reynolds number ($Re = 9000 - 18000 - 27000$), and two tests were performed with fixed Reynolds number ($Re = 18000$) in the trailing edge section, varying the outlet tip massflow rate from 12.5% to 25% of TE massflow.

To better investigate the effects of axial redirection of inlet radial flow, the results will be discussed in terms of the heat transfer coefficient distribution and mean values over the PS surface and they will be compared to the results from the corresponding axial geometries (Facchini and Tarchi [25]).

### Pressure Side Surface Heat Transfer

In Figs. 3 and 4, the PS surface heat transfer coefficient maps are presented for both the axial and the axial-radial configurations in order to compare the HTC distributions. In particular, in Fig. 3 the HTC distribution over the PS surface is presented in between two pedestals because in the axial configuration it is similar between each pair of pedestal.
As it can be seen comparing the aforementioned figures, the HTC scales are different: the maximum value for the axial configurations is one half of the corresponding one for the axial-radial geometries.

The presence of ribs causes a relevant increment of the turbulence level near the surface, then after each rib a noticeable increase of the heat transfer coefficient is present, see Fig. 3. The combined effect with flow acceleration leads to a generally increasing trend of HTC.

On the contrary in the baseline configuration $G1.0$, where the only flow acceleration effects are present, the heat transfer values are quite constant along the whole converging region. In particular, the map reveals a different behavior between the areas around the pedestals and the central part of the endwall: even if Mach number increases from 0.1 up to 0.3 in the region $L1$, at the midspan ($2 < y/D < 4$) the heat transfer coefficient increases slightly. Such behavior, due to the reduction of the turbulence level caused by the flow acceleration, is reported by other authors too [34].

Concerning the effect of the shape of the ribs on the heat transfer, the results globally shows a similar behavior of the square and the semicircular geometries.

The HTC surface maps for the axial-radial configuration are depicted in Fig. 4, referring to $Re = 18000$.

In the TE converging duct, downstream of the inlet constant duct there is a region of low HTC values corresponding to $-4 < y/S_y < -3$; this effect is expected to be caused by the presence of a recirculating region that is generated by the axial redirection to the TE of inlet radial flow where the flow separates from the wall corner while turning to the TE.

For the tip 0% configuration, which corresponds to no air stream flowing in the tip outlet section, in the tip constant height duct the HTC values are near to zero.

For tip 12.5% and specially for 25% configurations, it is possible to highlight a region of high HTC near tip outlet duct where a stagnation point is present: turbulence structures that arise in this area enhance local HTC.

With a closed tip section, in the region corresponding to $y/S_y > 2$ low HTC values are present due to a lack of massflow in this area for $G1.0$, $G1.1$ and $G1.2$; on the contrary, with 12.5% and 25% tip massflow rate, airflow distribution is expected to be more uniform compared to the previous case, producing a more uniform HTC distribution in the radial direction. Such a behavior produces lower HTC values for $y/S_y < -3$ for tip 0% condition.

Concerning pedestals, the axial-radial orientation of flowfield produces a non-uniform pressure distribution: on the lower surface, that will be referred as pedestal pressure side in the following for the sake of conciseness, pressure is higher while on the upper surface pressure is lower and will be referred as pedestal low pressure side.

Around pedestals, the surface heat transfer is higher but the distribution is not symmetrical around their axis due to flow mixed axial-radial orientation, as already stated. On the pressure side surface of elongated pedestals it is possible to highlight the presence of local HTC peaks generated by the interaction of the turbulent structures produced by the rib rows with the pedestal surfaces. On the low pressure side surface flow separates and creates a small recirculating region with again local low HTC values. Downstream of the first rib row it is also possible to point out a region of local HTC enhancement due the effect of the main air stream interacting with the pedestal leading edge and the first rib row.

**Spanwise Averaged HTC** In Fig. 5(a) the spanwise averaged surface heat transfer coefficient for $Re = 18000$ of the axial configuration [25] is presented; in the same figure the scheme of the PS surface is also presented to better understand the averaged spanwise HTC over $L1$ and $L2$. The main noticeable effect is the rib by rib HTC increase.

Moreover, the spanwise averaged HTC has a slight decrease starting from $x/D = 1$; this behavior as presented by many authors as [1] and [5] who showed the flowfield, is due to the recirculation before the first rib.
Downstream each rib is clearly visible a peak of the HTC, generated by the reattachment of the separated flow. Rib geometry also produces some relevant differences on HTC peak values: square ribs produce higher turbulence comparing to semicircular ones so they experience higher averaged HTC values.

In the axial-radial configuration (see Fig. 5(b)), for the baseline geometry $G1.0$ there is a slight increase of the HTC downstream of the pedestal leading edge ($x/D = 2$); in fact, differently from the axial geometry, the air stream entering the TE section is expected to be not fully axial because of its radial velocity component and consequently the stagnation point does not correspond to pedestal leading edge.

With an open tip section the averaged spanwise HTC values are higher over the $L1$ region and similar for both square and semicircular ribs.

Over $L1$, the averaged HTC increases row by row and its values are higher than those experienced in the axial configuration. This behavior is also affected by the interaction of the turbulent structures generated in the main air stream row by row with the pedestal surfaces; this behavior is related to the radial velocity component of the flow turning to the TE.

It is also worth noting that the averaged HTC peak generated by the third row of rib is located at $x/D = 10$, that corresponds to the trailing edge throat section where, as stated in the previous paragraph, the turbulence generated by the ribs is lowered.

For the axial configuration, the HTC peak values downstream of the first two rib rows are located at different positions comparing square and semicircular ribs while the third peak is placed at same $x/D$. On the contrary for the axial-radial configuration HTC peak values are placed at the same position downstream of each rib row. In this configuration the airstream flowing in between the pedestals and the turbulent structures generated by the rib rows interacts with the pedestal surfaces, unlike the axial configuration.

About different tip massflow rates, the main effect consists in HTC enhancement, while peak values are located at the same position.

Over the $L2$ region, the effect of the rib shape and of the tip flow on the averaged HTC is not noticeable.

## AVERAGED NUSSELT VALUES OVER THE P.S. SURFACE IN THE REGION $L0$, $L1$ AND $L2$.

***L0* region Nusselt values.** As depicted in Fig. 6(a), the average Nusselt number for the axial configurations evaluated in the inlet section is in line with the Colburn correlation for turbulent fully developed flows in straight ducts.

In both axial and axial-radial configurations there are no significant differences between the two ribbed geometries because the flowfield in $L0$ is not affected by pedestals and ribs position.

Surface Nusselt values of the axial-radial configuration are different from the axial one because of the higher flow velocity that enters the $L0$ region from the hub inlet. As stated before, both Reynolds and Nusselt numbers are always calculated referring to the $L1$ inlet region ($x/D = 0.0$) duct dimensions of the axial geometry.

***L1* region Nusselt values.** In the region $L1$, see Fig. 6(b), $G1.1$ and $G1.2$ experience a similar averaged behavior showing that the rib geometry has a slight effect on the mean Nusselt number, even though the effect on HTC distribution is noticeable, as previously mentioned.

Moreover, there is no remarkable influence of the tip massflow rate and consequently the $\overline{Nu}_{L1}$ values are similar with closed or open tip section, even though HTC distribution has a different behavior.

***L2* region Nusselt values.** In the $L2$ region, see Fig. 6(c), only the increase of flow Reynolds number produces an increase of mean $Nu_{L2}$: considering the tested flow conditions, the effects of turbulence enhancement due to rib rows and flow orientation are strongly reduced at $L1$ outlet section, corresponding to $x/D = 10$ in Fig. 4.

As in the $L1$ region, even though the HTC distribution over the $L2$ surface is not uniform for different tip massflow rates as stated in the previous paragraphs, globally the mean value is not affected.

## Pressure Drop

The experimental survey performed on geometries $G1.0$, $G1.1$ and $G1.2$ was completed evaluating the friction factor, defined in Eq. 4 and shown in Fig. 7, for all the tested conditions.

From Fig. 7, at a low Reynolds number the differences between the friction factor calculated for the three geometries is negligible while for higher Reynolds number, as expected, the lower values of the pressure drop was measured for the baseline geometry $G1.0$.

In geometries $G1.1$ and $G1.2$, the pressure drop increase is due to the effect of turbulators that causes flow separations, recirculations and reattachments combined with flow acceleration produced by the reduction of cross sectional area; this effect is particularly evident near the throat section where the area con-

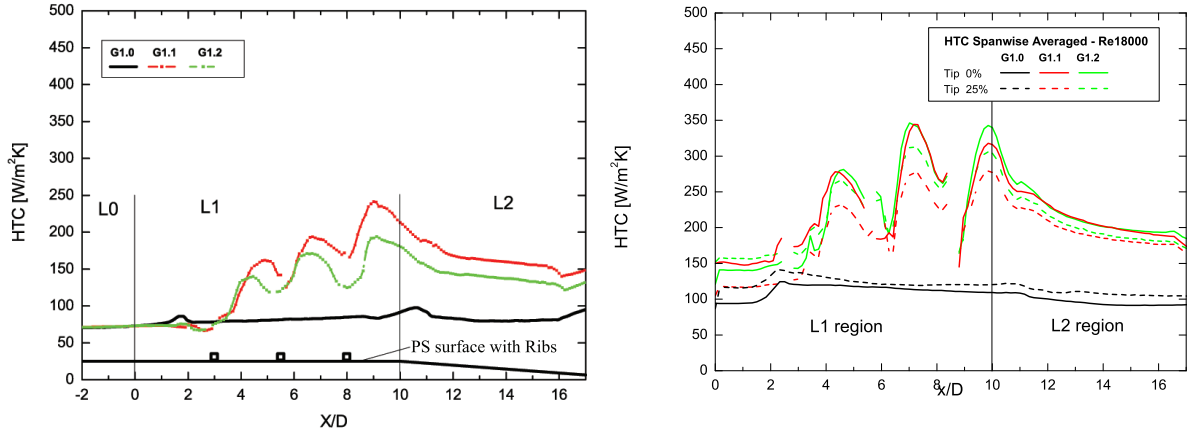


(a) Spanwise Averaged HTC - Axial Configuration

(b) Spanwise Averaged HTC - Axial-Radial Configuration

Figure 5. SPANWISE AVERAGED HEAT TRANSFER COEFFICIENT - L1 REGION - $Re = 18000$

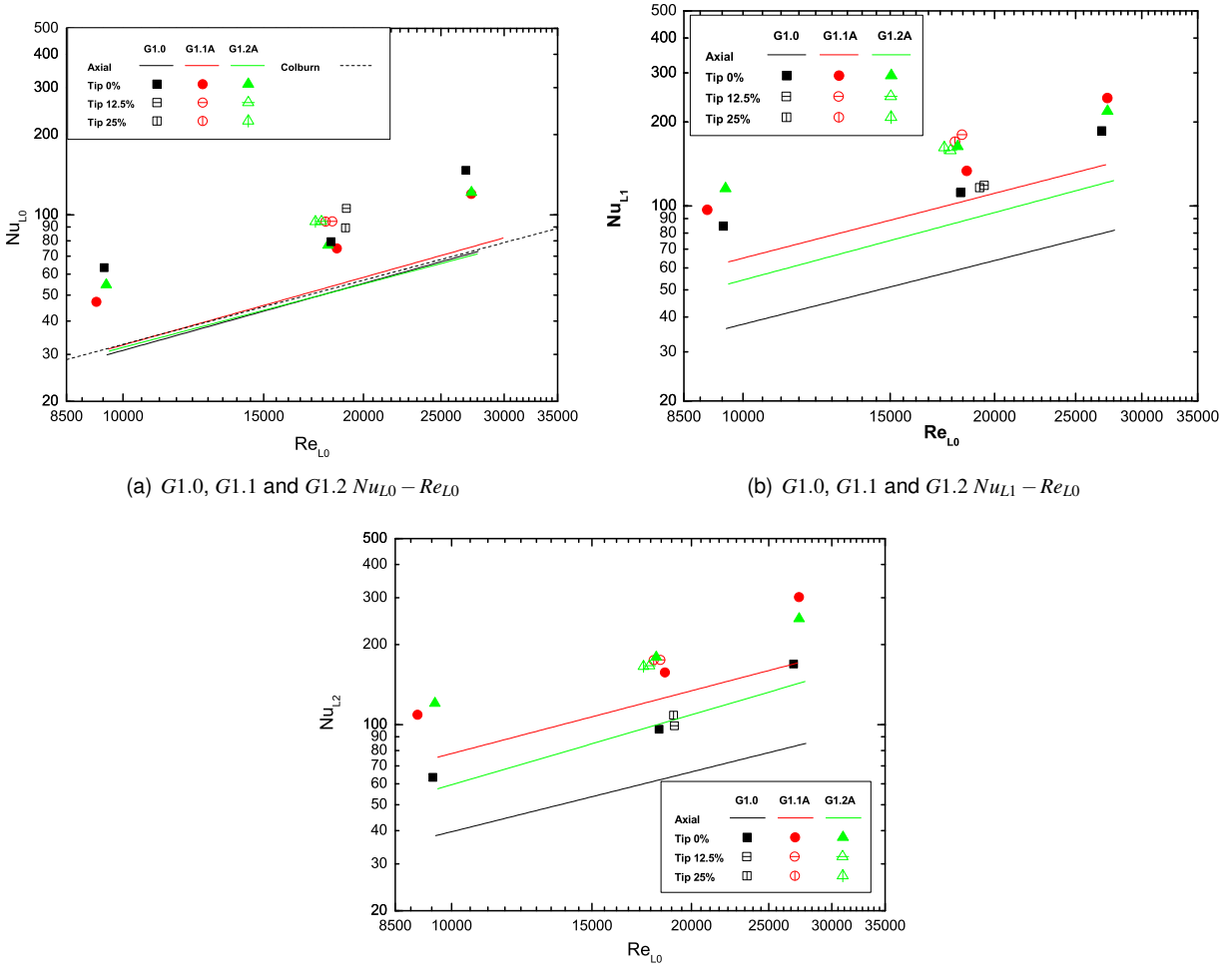


(a) $G1.0$, $G1.1$ and $G1.2$ $Nu_{L0} - Re_{L0}$

(b) $G1.0$, $G1.1$ and $G1.2$ $Nu_{L1} - Re_{L0}$

(c) $G1.0$, $G1.1$ and $G1.2$ $Nu_{L2} - Re_{L0}$

Figure 6. AVERAGED NUSSELT NUMBER VALUES OVER THE REGIONS $L0$, $L1$ AND $L2$ for $G1.0$, $G1.1$ AND $G1.2$ FOR THE AXIAL AND AXIAL-RADIAL CONFIGURATIONS

traction is higher. As a consequence, friction factor difference between $G1.0$ and $G1.1$ or $G1.2$ is more and more evident from $Re = 9000$ to $Re = 27000$.

For the open tip section conditions, the pressure drop slightly changes with an increase of the tip massflow rate.

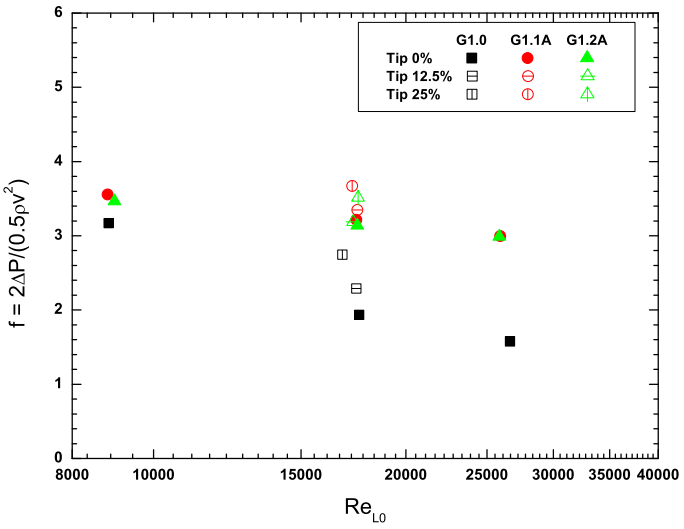


Figure 7. COMPARISON OF $f$ BETWEEN THE GEOMETRIES $G1.0$, $G1.1$ AND $G1.2$ FOR THE AXIAL-RADIAL CONFIGURATIONS

## CONCLUSIONS

In the present article, an experimental investigation concerning heat transfer and pressure drop was performed taking into account the combined effect of elongated pedestal arrays with and without fillet radius and ribs in a wedge shaped duct for axial-radial trailing edge cooling system geometries. In $G1.1$ and $G1.2$, the effects of square and semicircular ribs were investigated comparing to the baseline configuration $G1.0$ without ribs. Five tests were performed: tests with tip flow were performed at $Re = 18000$ keeping constant the TE massflow rate and Mach number and varying tip massflow. The experimental survey was carried out with the transient TLC technique in order to measure detailed heat transfer coefficient maps over the pressure side surface.

In order to highlight the effects of rib rows, HTC results have been presented and discussed in terms of bidimensional maps, averaged spanwise HTC distribution over $L1$ and $L2$ and mean Nusselt values over $L0$, $L1$ and $L2$ regions, also comparing to results from the axial configuration of the same test article.

Pressure drop were evaluated in adiabatic conditions, defining a friction factor that depends on the total pressure drop between the hub inlet and TE outlet section.

In the investigated test articles axial redirection of inlet radial flow causes several relevant effects on the flowfield and mainly on HTC distribution and mean values over the $L1$ PS surface.

In fact, for tip 0% condition radial distribution of the heat transfer coefficient is non uniform and the HTC is lower in the region near the tip outlet. For tip 12.5% and 25% configuration the HTC distribution is more uniform for both $G1.1$ and $G1.2$ geometries and no significant differences between rib shapes can be highlighted.

Comparing the baseline geometry $G1.0$ with $G1.1$ and $G1.2$, the influence of ribs is remarkable in terms of both spanwise averaged HTC and mean $Nu$ values over $L1$ and $L2$; in fact downstream each rib row HTC increases due to the high turbulence level and the interaction with pedestal surfaces. However, downstream of the third rib row the aforementioned effect is not present and spanwise averaged augmentation is limited, while in the axial configuration HTC increases row by row.

Unlike the axial configuration, turbulence generated by ribs interacts with pedestal surfaces causing a high increase of HTC near pedestal surfaces, while HTC distribution around pedestal axis is not symmetrical due to mixed axial-radial flow.

As far as mean Nusselt number values are concerned, the enhancement of $Nu_{L0}$ comparing to the axial configuration is due to the higher flow velocity and the augmentation concerning tip 12.5% and 25% conditions is caused by the increase of massflow rate compared to tip 0% configuration. In $L1$ region HTC enhancement due to rib rows is nearly independent from rib geometry.

About the pressure drop, the effect of rib rows is noticeable in both test article configurations; comparing to the baseline geometry, turbulators cause the overall increase of the pressure drop. The contribution of the square and semicircular ribs is similar and the difference of friction factor compared to the baseline geometry increases with the Reynolds number.


## Acknowledgments

The reported work was performed within the European research project *AITEB2 - Aerothermal Investigation of Turbine Endwalls and Blades* (RTD-Project $6^{th}$ FP, Contract No.AST4-CT-2005-516113). The permission for the publication is gratefully acknowledged by the authors.


## REFERENCES


[1] Han, J. C., Dutta, S., and Ekkad, S. V., 2000. *Gas Turbine Heat Transfer and Cooling Technologies*. Taylor & Francis.

[2] Hwang, J. J., and Lui, C. C., 2002. "Measurement of endwall heat transfer and pressure drop in a pin-fin wedge duct". *International Journal of Heat and Mass Transfer,* **45**, pp. 877–889.

[3] Carcasci, C., Facchini, B., and Innocenti, L., 2003. "Heat transfer and pressure drop evaluation in thin wedge-shaped trailing edge". *ASME Paper*(GT2003-38197).

[4] Facchini, B., Innocenti, L., and Tarchi, L., 2004. "Pedestal and endwall contribution in heat transfer in thin wedge shaped trailing edge". *ASME Paper*(GT2004-53152).

[5] Han, J. C., Park, J. S., and Lei, C. K., 1985. "Heat transfer enhancement in channels with turbulence promoters". *ASME Journal of Engineering for Gas Turbine and Power,* **107**, pp. 628–635.

[6] Han, J. C., 1988. "Heat transfer and friction characteristics in rectangular channels with rib turbulators". *ASME Journal of Heat Transfer,* **110**, pp. 321–328.

[7] Han, J. C., and Park, J. S., 1988. "Developing heat transfer in rectangular channels with rib turbulators". *ASME Journal of Heat and Mass Transfer,* **31**, pp. 183–195.

[8] Chandra, P. R., and Cook, M. M., 1994. "Effect of the number of ribbed walls on heat transfer and friction characteristics of turbulent flows". *ASME HTD General Papers in Heat and Mass Transfer,* **271**, pp. 201–209.

[9] Chandra, P. R., Niland, M. E., and Han, J. C., 1997. "Turbulent flow heat transfer and friction in a rectangular channel with varying number of ribbed walls". *ASME Journal of Turbomachinery,* **119**, pp. 374–380.

[10] Taslim, M. E., and Spring, S. D., 1994. "Effects of turbulator profile and spacing on heat transfer and friction in a channel". *Journal Of Thermophysics And Heat Transfer,* **8**(3).

[11] Taslim, M. E., and Nezym, V., 2007. "A new statistical-based correlation for the rib fin effects on the overall heat transfer coefficient in a rib-roughened cooling channel". *International Journal of Rotating Machinery,* **2007**(68684).

[12] Burggraf, F., 1970. "Experimental heat transfer and pressure drop with two dimensional turbulence promoters applied to two opposite walls of a square tube". *ASME, Augmentation of Convective Heat and Mass Transfer*, pp. 70–79.

[13] Chandra, P. R., and Han, J. C., 1989. "Effects of turbulator profile and spacing on heat transfer and friction in a channel". *Journal of Thermophysics and Heat Transfer,* **3**(3), pp. 315–319.

[14] Cakan, and Arts, T., 1999. "Effect of main and secondary flows on heat transfer in a rib-roughned internal cooling channel". *4th International Symposium on Experimental and Computational aerothermodynamics of Internal Flows*(VKI-RP 1999-42).

[15] Kiml, R., Mochizuki, S., and Murata, A., 2001. "Effects of rib arrangements on heat transfer and flow behavior in a rectangular rib-roughened passage: Application to cooling of gas turbine trailing edge". *Journal of Heat Transfer,* **123**, pp. 675–681.

[16] Liou, T. M., Wu, Y. Y., and Chang, Y., 1993. "Ldv measurements of periodic fully developed main and secondary flows in a channel with rib-disturbed walls". *Journal of Fluids Engineering,* **115**, pp. 109–114.

[17] Hwang, J. J., and Lui, C. C., 1999. "Detailed heat transfer characteristic comparison in straight and 90-deg turned trapezoidal ducts with pin-fin arrays". *International Journal of Heat and Mass Transfer,* **42**, pp. 4005–4016.

[18] Kulasekharan, N., and Prasad, B., 2008. "Effect of coolant entry orientation on flow and heat transfer in the trailing region channels of a gas turbine vane". *ASME*(GT2008-50951).

[19] Liu, Y. H., Huh, M., Wright, L. M., and Han, J. C., 2008. "Heat transfer in trailing edge, wedge shaped cooling channels with slot ejection under high rotation numbers". *ASME*(GT2008-50343).

[20] Wang, Z., Ireland, P. T., and Jones, T. V., 1993. "Detailed heat transfer coefficient measurements and thermal analysis at engine conditions of a pedestal with fillet radii". *ASME Paper*(93-GT-329).

[21] Wang, Z., Ireland, P. T., Jones, T. V., and Kohler, S. T., 1994. "Measurements of local heat transfer coefficient over the full surface of a bank of pedestals with fillet radii". *ASME Paper*(94-GT-307).

[22] Hwang, J. J., and Lui, C. C., 2000. "Lateral-flow effect on endwall heat transfer and pressure drop in a pin-fin trapezoidal duct of various pin shapes". *ASME Paper*(2000-GT-0232).

[23] Facchini, B., Tarchi, L., and Zecchi, S., 2008. "Experimental investigation of innovative internal trailing edge cooling configurations with pentagonal arrangement and elliptic pin fin". *12th ISROMAC Symposium, 17-22 February 2008, Honolulu, Hawaii, Paper ISROMAC*$12-2008-20089$.

[24] Chen, S. P., Li, P. W., Chyu, M. K., Cunha, F. J., and Abdel-Messeh, W., 2006. "Heat transfer in an airfoil trailing edge configuration with shaped pedestals mounted internal cooling channel and pressure side cutback". *ASME Paper*(GT2006-91019).

[25] Facchini, B., and Tarchi, L., 2008. "Investigation of innovative trailing edge cooling configurations with enlarged pedestals and square or circular ribs. part i - experimental results". *ASME Paper*(GT2008-51047).

[26] Bacci, A., Facchini, B., Innocenti, L., and Tarchi, L. "Combined use of turbulators and enlarged pedestals in trailing edge cooling systems: an experimental and numerical analysis". *6th ETC Conference, 7-11 March 2005, Lille, France,* **078-04/94**.

[27] Di Carmine, E., Facchini, B., and Mangani, L., 2008. "Investigation of innovative trailing edge cooling configurations with enlarged pedestals and square or circular ribs. part ii - numerical results". *ASME Paper*(GT2008-51048).

[28] M.Rosenhow, W., and Hartnett, J. P., 2000. *Handbook of Heat Transfer*. Mc Graw Hill Inc.

[29] Ireland, P. T., Wang, Z., and Jones, T. V., 1993. "Liquid crystal heat transfer measurements". In *Measurements Techniques*, Lecture Series 1993-05. von Karman Institute for Fluid Dynamics.

[30] Camci, C., 1995. "Liquid crystal thermography". In *Temperature Measurements*, Lecture Series 1996-07. von Karman Institute for Fluid Dynamics.

[31] Ireland, P. T., and Jones, T. V., 2000. "Liquid crystal measurements of heat transfer and surface shear stress". *Measurement Science Technology,* **11**, pp. 969–986.

[32] ASME, 1985. "Measurement uncertainty". In *Instrument and Apparatus*, Vol. ANSI/ASME PTC 19.1-1985 of *Performance Test Code*. ASME.

[33] Kline, S. J., and McClintock, F. A., 1953. "Describing uncertainties in single sample experiments". *Mechanical Engineering,* **75**, Jen, pp. 3–8.

[34] Metzger, D. E., Shepard, W. B., and Haley, S. W., 1986. "Row resolved heat transfer variations in pin-fin arrays including effects of non-uniform arrays and flow convergence". *ASME Paper*(86-GT-132).